River transport effects on compressional belts: fist results from an integrated analogue-numerical model.

Persson, K.S.; Garcia-Castellanos, D.; Sokoutis, D.

published in
Journal of Geophysical Research. Solid Earth
2004

DOI (link to publisher)
10.1029/2002JB002274

document version
Publisher's PDF, also known as Version of record

River transport effects on compressional belts: First results from an integrated analogue-numerical model

Katarina S. Persson
Geological Survey of Sweden, Uppsala, Sweden

Daniel Garcia-Castellanos and Dimitrios Sokoutis
Netherlands Centre for Integrated Solid Earth Science, Faculty of Earth and Life Sciences, Vrije Universiteit Amsterdam, Amsterdam, Netherlands

Received 30 October 2002; revised 5 September 2003; accepted 23 October 2003; published 17 January 2004.

[1] Erosion, deposition, and tectonic processes interact to define the style of deformation in compressional belts. This paper introduces a method of integrating a numerical model for surface transport with analogue sandbox models of compressional belts to further improve our understanding of this interplay. The analogue model provides the numerical model with the rising topography, whereas the numerical model calculates the river network and the resulting amount of erosion and sediment transport. Compared to previous analogue models with uniform (two-dimensional) erosion this method provides a tool to incorporate process-based rates of erosion and deposition with spatial distributions that depend on the river network developed on the evolving topography. Rivers running parallel to the evolving mountain belt induce along-strike changes in erosion and deposition that in turn result in asymmetric tectonic deformation. The additional load of sediments controls the propagation of thrust as well as the direction of vergence of the main thrust. High erosion rates do not always lead to fewer thrusts within the compressional belts but generally steepen and lengthen the lifetime of the affected faults. *INDEX TERMS:* 8102 Tectonophysics: Continental contractional orogenic belts; 1815 Hydrology: Erosion and sedimentation; 8010 Structural Geology: Fractures and faults; 3210 Mathematical Geophysics: Modeling; 3344 Meteorology and Atmospheric Dynamics: Paleoclimatology; *KEYWORDS:* orogens, erosion, sedimentation, sandbox

Citation: Persson, K. S., D. Garcia-Castellanos, and D. Sokoutis (2004), River transport effects on compressional belts: First results from an integrated analogue-numerical model, *J. Geophys. Res.*, *109*, B01409, doi:10.1029/2002JB002274.

1. Introduction

[2] It has long been understood that tectonic uplift controls the atmosphere and ocean circulations and therefore also the global climate, which in turn affects the physical weathering and erosion [*Ruddiman*, 1997, and references therein]. However, over the last fifteen years it has become clear that erosion on the other hand can have a significant impact on the tectonic evolution of compressional belts. This has resulted in a number of papers using both analogue and numerical modeling techniques to study the interplay between surface and crustal-scale processes. Numerical models have demonstrated that syntectonic erosion affects the critical state of the orogenic wedge and that the dynamics between tectonics and erosion contain important feedback mechanisms such that orogenic systems tend toward a steady state [*Jamieson and Beaumont*, 1988, 1989; *Willett*, 1999; *Willett and Brandon*, 2002]. The dramatic effects of erosion on the evolution of the internal structure of the Swiss Alps have been discussed on the basis of numerical models by *Pfiffner et al.* [2000]. A thermal-mechanical numerical model has also linked ductile extrusion and channel flow of high-grade metamorphic rocks in the Himalayas to surface denudation localized to the edge of a plateau that is underlain by low-viscosity material [*Beaumont et al.*, 2001]. Analogue models have revealed a number of changes induced by erosion in tectonic deformation within the wedge, such as the amount of lithospheric thickening [*Davy and Cobbold*, 1991], fault reactivation [*Leturmy et al.*, 2000], longer lived thrusts leading to steepening of the faults [*Cobbold et al.*, 1993; *Merle and Abidi*, 1995], and a decrease in the importance of effective indenters [*Persson and Sokoutis*, 2002]. Erosion by surface transport has also been proposed to prevent collapse of an intracontinental range as removal of material from topographic heights and deposition in the foreland oppose spreading of the crustal root [*Avouac and Burov*, 1996]. Field studies also show the control that erosion exerts on tectonic processes, revealing higher exhumation rates along faults in areas subject to severe erosion [*Koons*, 1990; *Hoffman and Grotzinger*, 1993; *Norris and Cooper*, 1997].

[3] In addition to the effects of erosion, loading by sediment deposition in front of the orogen induces forward

0148-0227/04/2002JB002274$09.00

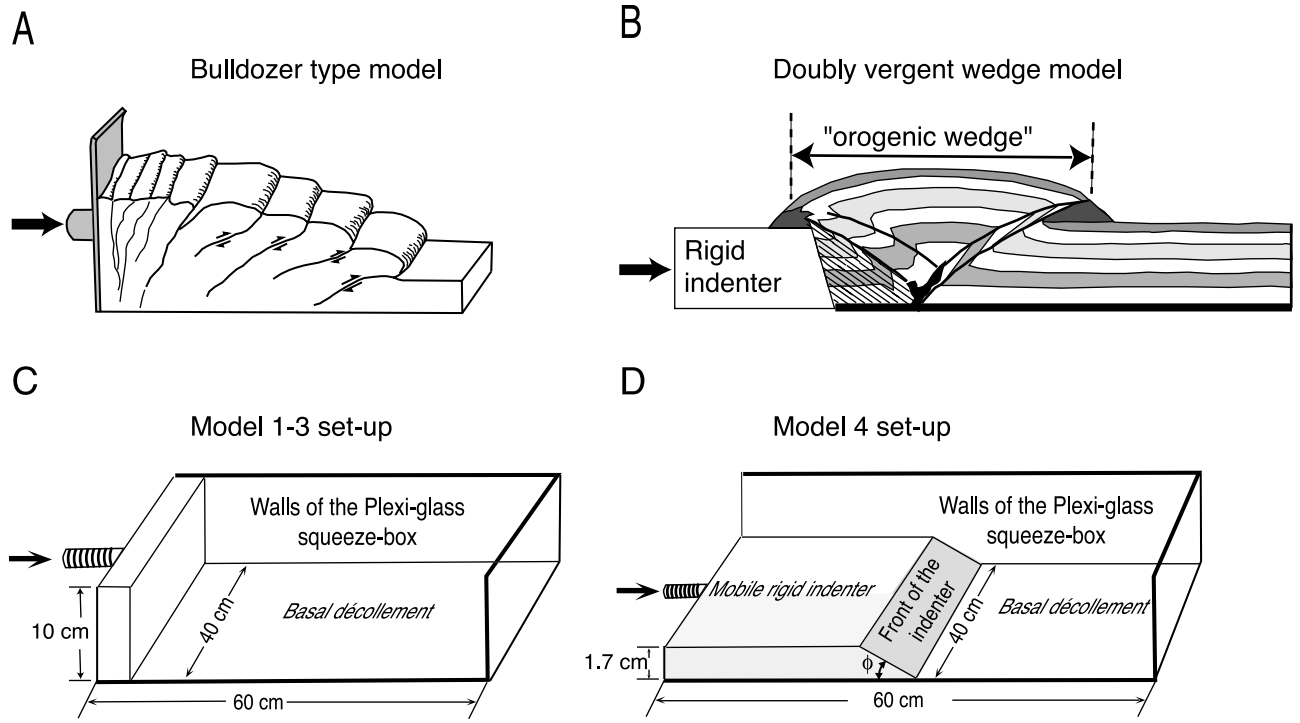

Figure 1. (a) Bulldozer-type model [e.g., *Davis et al.*, 1983]. A vertical backstop is pushed into the sand resulting in a one-sided wedge as sand is only allowed to spread in one lateral direction (forward). (b) Doubly vergent-type model [cf. *Koons*, 1990; *Beaumont et al.*, 1992; *Bonini et al.*, 1999; *Persson*, 2001]. A rigid indenter originally of the same height as the sand is used, resulting in a doubly vergent wedge where sand is allowed to spread both over the indenter as well as over the indented sand. (c) Setup for models 1–3 with a vertical bulldozer-type indenter. (d) Setup for model 4 with a rigid indenter of 30°. Arrows indicate the movement of the rigid indenter.

propagation of thrusting [*Cobbold et al.*, 1993; *Mugnier et al.*, 1997; *Leturmy et al.*, 2000; *Persson and Sokoutis*, 2002]. However, previous analogue models have been simplistic in assuming constant erosion rates that do not vary along the orogen axis. They therefore fail to account for the axial (orogen parallel) direction of transport and variations of erosion rate over time observed in many orogen-basin systems [e.g., *Schlunegger et al.*, 2001]. In reality, rivers are responsible for most mass transport from orogen to basin [e.g., *Gupta*, 1997] and introduce spatial changes in erosion/sedimentation rates [cf. *Garcia-Castellanos*, 2002]. These variations are likely to affect the evolution of analogue models. Inversely, the location of river basins is the result of the topography induced by tectonic processes, suggesting a possible feedback between tectonism and the distribution of erosion and sedimentation determined by river basins. Whereas analogue models provide an efficient tool to study the dynamics of lithospheric deformation, existing numerical models of surface erosion and sediment transport provide quantitative approaches to the spatial redistribution of the erosion products over time.

[4] This paper presents a combined numerical and analogue technique in which a sandbox model is used to simulate the dynamics of tectonic deformation in the upper crust and a numerical fluvial transport model simulates the dynamics of erosion and deposition. This technique takes into account the three-dimensional (3-D) feedback effects described above and provides a new tool to address the interplay between tectonic response and surface mass transport.

2. Analogue Model Setup

[5] Well-rounded dry quartz sand $\leq$0.297 mm in diameter, a Mohr-Coulomb material [*Byerlee*, 1978] with a density for sieved sand of 1510 kg/m^3, and a mean angle of internal friction of 44° (or a coefficient of friction of 0.97) were used to represent the brittle behavior of the upper continental crust. The sand was sieved into a Plexiglas sandbox with horizontal dimensions of 40 $\times$ 60 cm and a layer thickness of 1.6 cm. A color stratigraphy in the sand was used to visualize the deformation in profile. The cohesion (T_0) of rocks has the dimensions of stress; thus $\tau^* = \sigma^*$, where the stress ratio $(\sigma^*) = \rho^* g^* L^*$ [*Weijermars and Schmeling*, 1986]. An average density of 2700 kg/m^3 for the crystalline upper crust gives a density ratio (ρ^*) of $\sim$0.56 and a gravity ratio (g^*) of 1 between the model and nature. The measured cohesion of the sieved sand was 69 Pa. Cohesion of natural rocks are within the range of 0–70 MPa [*Goodman*, 1989]. This implies a length ratio between 10^{-4} and 10^{-6} justifying the scaling used for the analogue model of 1 mm:1000 m. The basal friction coefficient between the sand and the bottom of the squeeze box was $\sim$0.4.

[6] Both bulldozer-type models (Figure 1a) for individual fold-and-thrust belts and accretionary prisms [e.g., *Davis et*

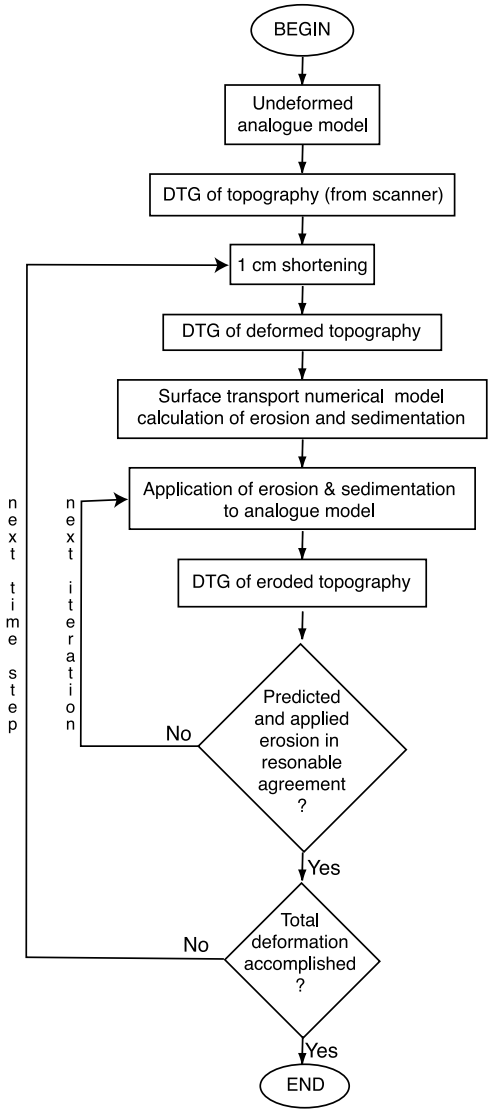

Figure 2. Methodology scheme of the integration between the analogue and the numerical model. DTG stands for digital topographic grid. Each time step consists of 1 cm shortening in the sandbox, followed by the numerical calculation of erosion/sedimentation distribution on top of the modified topography and the application of this prediction to the analogue model.

al., 1983] as well as doubly vergent-type models (Figure 1b) of orogenic wedges [cf. *Koons*, 1990; *Beaumont et al.*, 1992; *Bonini et al.*, 1999] are presented in this paper. In the bulldozer-type models, a vertical backstop higher than the indented sand is used to push a sand-pack in one lateral direction without allowing the sand to spread over the indenter leading to one-sided wedge geometry. In models where indenters are of the same vertical dimension as the indented sand, a doubly vergent wedge develops as the sand is allowed to spread both over the indenter as well as over the indented continent. The two different boundary conditions results in very different internal thrust geometries. The models presented in this paper are not of any specific area but are designed to study the methodology in integration of analogue and numerical modeling techniques. Therefore we have chosen to test both types of model setups (Figure 1).

[7] In models 1–3 a vertical wall (backstop) was used, whereas in model 4 an indenter with an angle of 30° and the same vertical thickness as the sand was used. The indenter in all experiments was driven into the sand-pack with a speed of 26 mm/h (Figures 1c and 1d). However, the rate of displacement does not need to be scaled because Coulomb materials have a yield envelope essentially independent of strain rate [*Kusznir and Park*, 1984a, 1984b; *Sonder and England*, 1986].

[8] The model did not account for the formation of a flexural basin (a topographic depression) in front of the compressional belt by isostasy (compare models by *Davy and Cobbold* [1991] and *Cobbold et al.* [1993]). A "basin" was introduced by slightly tilting the box (~0.5°) toward the indenter in all models. This initial tilt was necessary to localize topographic minima and sedimentation in front of the compressional belt, simulating the tilt produced by lithospheric flexure. Time-dependent tilting of the box has previously been used by others [*Leturmy et al.*, 2000]. However, our model was tilted once at the start and no further tilting was added because we focused on the effects of erosion on tectonics rather than the role of flexure. This means that the results below will account for the interplay between the wedge internal deformation and the surface processes, but not for the possible role of lithospheric flexure in this interplay.

[9] The initially undeformed surface was scanned with a 3-D video laser to produce a digital topographic grid (DTG) of the model surface. The DTG was set to a vertical resolution of 0.1 mm and a horizontal spacing of 0.5 mm. After 1 cm of lateral shortening of the model (2 Myr), the new topography was scanned and the change of topography was achieved by subtracting the initial surface DTG from the new one. A convergence rate of 5 mm/yr is set as a representative figure for continental collision (e.g., *Schmid et al.* [1996] derive convergence rates of 7 mm/yr on a timescale of 65 Myr in the Swiss-Italian Alps). The resulting file showing the change in elevation was used as input to the numerical surface transport model (Figure 2). In turn, the numerical model calculated the river network as well as the resulting spatial distribution of erosion and sedimentation (see below).

[10] The analogue model was then eroded, with a vacuum cleaner fitted with a fine nozzle, until the erosion was close to that shown on the map of surface transport. The collected sand was weighed. The sand deposited (in the amount calculated by the numerical model) was of another color to remain clearly visible in the profiles. The obtained new surface was scanned to produce a new DTG. The erosion/sedimentation increment was calculated from the DTG before and after the erosion of the analogue model. The accumulated erosion/sedimentation was compared to the accumulated erosion according to the numerical model. Erosion was repeated until the erosion in the analogue model was close to the one predicted in the numerical model. This procedure was repeated at steps of 1 cm of shortening (Figure 2). The resulting model evolutions are displayed later in this paper. The tilt of the models was induced before the first top surface DTG was produced. The

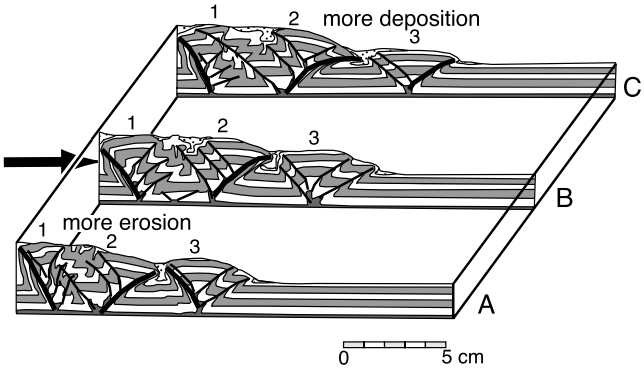

Figure 3. Cross sections (A–C) of model 1 after 11 cm shortening (22 Myr). Shaded and open layers are the deformed stratigraphy, whereas the dotted pattern represents sediment. Thickness of lines indicates the relative importance of each thrust. Deformation along profile C, where more sedimentation and less erosion takes place, has propagated further forward compared to the other profiles. The arrow indicates the movement of the rigid indenter (backstop). Numbers (1, 2, and 3) indicate the sequence of formation of the pop-up structures.

lowest area of the scanned initial topography was taken to be a zero level (0 elevation) and the initially higher areas were shown by positive values of the elevation.

3. Surface Transport Model

[11] To calculate erosion and deposition on top of the dynamic topography generated by the analogue model, surface sediment transport is calculated via a numerical model of fluvial transport (see *Garcia-Castellanos* [2002] for further details). This model assumes that sediment transport is driven by rivers in which equilibrium transport capacity q^{eq} (measured in kg per second) is linearly proportional to their water discharge Q_w and channel slope S along the river (e.g., the stream power approach of *Kooi and Beaumont* [1996]):

$$q^{eq} = K_f S Q_w, \tag{1}$$

where K_f is a constant measured in kilograms of sediment per cubic meter water discharge. The amount of erosion/deposition at each location dq is in turn proportional to the difference between the actual sediment load and the equilibrium transport capacity.

$$\frac{dq}{dl} = -\frac{1}{l_f}(q - q^{eq}), \tag{2}$$

where dl is a length increment along the river path and l_f is a parameter defining the length scale at which the river achieves transport equilibrium. We use l_f = 120 km for the bedrock and l_f 60 km for the sediments. Within this approach, a river can change from incision to aggradation by a decrease in discharge and/or slope. Although other relationships have been proposed to explain the transition from incision along rivers to aggradation [e.g., *Howard*, 1994; *Tucker and Slingerland*, 1997; *Whipple and Tucker*, 1999], the differences are not substantial for our purposes in the sense that all of them reproduce the basic properties of rivers as transport agents (e.g., effect of base level changes, equilibrium river profile, dynamic equilibrium topography, hierarchical organization of the river network, etc. [*Kooi and Beaumont*, 1996]).

[12] Equations (1) and (2), relating water discharge, slope, and erosion/deposition rate are solved using the finite difference method and using the same square mesh digitized from the analogue model. To convert erosion/deposition rates into eroded/deposited thickness, we assume that each time step corresponds to 2 Myr (implying a shortening rate of 5 km/Myr). For the purpose of the erosion/sedimentation calculations, we use a vertical scale factor of 1 mm:300 m in order to avoid unrealistic high topography. Note that the model does not incorporate isostatic compensation, thus overestimating the topography in the model. This scaling factor is within the range discussed in section 2.

[13] Rainfall is given a constant value throughout the model and water is transferred from cell to cell following the steepest downward direction. The model accounts for the formation of lakes in local topographic minima. For simplicity, we disregard evapotranspiration, which implies that all lakes are open (have at least one outlet) and drain out all the water they receive from tributaries plus the local rainfall on the lake. As a river reaches the shore of a lake or the sea, sediments are distributed throughout the water body in all directions from the river mouth and deposited assuming a rate decreasing exponentially with the distance from the mouth. Hillslope (diffusive) transport, dominant only over distances of few km or less, has been disregarded, since our paper focuses on the effects produced by large-scale (fluvial) transport.

[14] This erosion-transport-sedimentation model is mass conservative: all eroded material is either deposited within the model or driven out of the boundaries of the model domain.

4. Model Results

4.1. Model 1

[15] Relief-dependent mechanisms of erosion, such as fluvial incision and mass wasting (e.g., landsliding, avalanches, etc.) [*Ahnert*, 1970], lead to high erosion rates in mountain belts with high relief. Increased elevation can also lead to high erosion rates by orographic enhancement of precipitation rates [*Barry*, 1981]. To explore if high erosion rates would create structural variations along the strike of the compressional belt, orogen erosion was enhanced on the higher half of the model (between sections A and B in Figure 3). Additionally, sedimentation was concentrated in front of the model orogen on the initially lower side (between sections B and C in Figure 3). Model 1 was designed as a pilot model in which the numerical prediction of the surface transport was used just to determine the areas of erosion and deposition whereas their absolute magnitude were not applied with precision to the analogue model. During this experiment, the side undergoing higher erosion rates retained its high

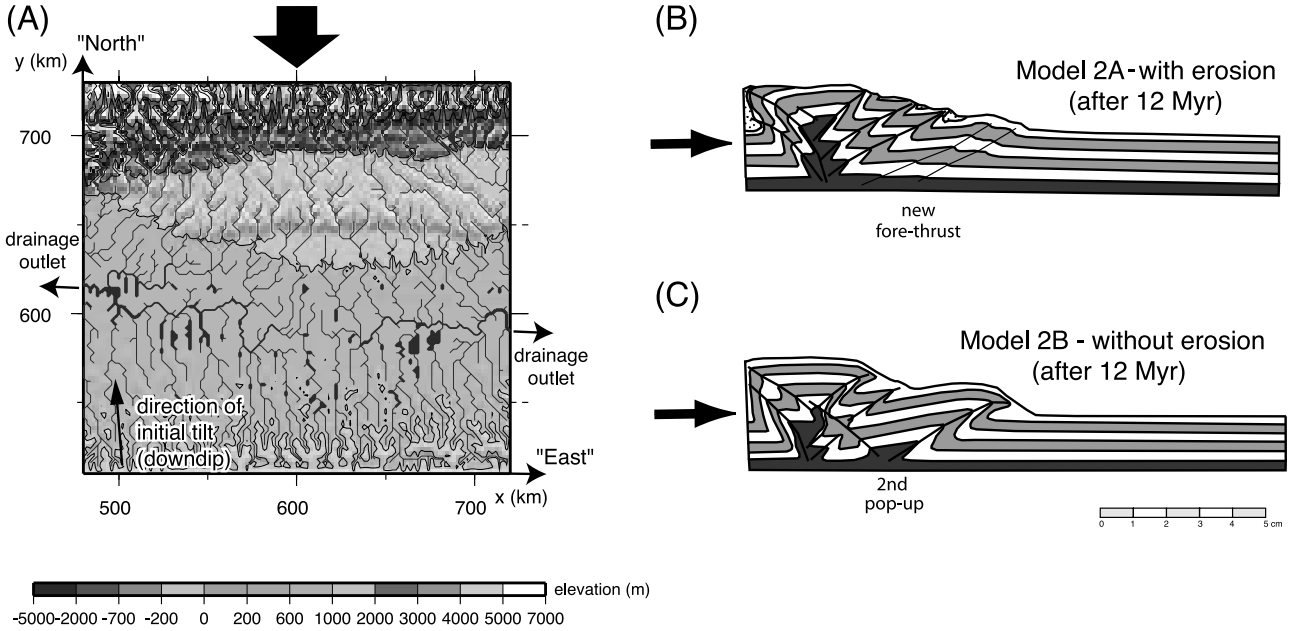

Figure 4. Last stage of the evolution of model 2, after 6 cm (equivalent to 60 km shortening and 12 Myr). (a) Top view of the analogue model topography (model 2A) and drainage pattern resulting from the numerical model. Main drainage directions on the foreland are indicated. The initial topography corresponds to a plane slightly tilted (0.5°) toward the upper left direction. (b) Section of the sand model 2A with erosion and (c) model 2B without erosion. Thick arrows indicate the movement of the rigid indenter.

elevation by reverse faulting: sand was transferred at a high rate along its long-lived faults. At the same time, these faults were rotated and steepened [cf. *Cobbold et al.*, 1993].

[16] After 11 cm shortening (22 Myr) the model orogen developed clear structural differences along strike. Three pop-up structures are seen in all the profiles (Figure 3). However, on the side of the compressional belt that was subjected to higher erosion rates and lower amounts of deposition (profile A in Figure 3), the width of the model orogen is smaller than on the side of the belt with less erosion but more deposition (profile C in Figure 3). The faults are also steeper along profiles that have suffered higher erosion rates. The main fault (thick line in Figure 3) of the last developed pop-up structure (pop-up 3 in Figure 3) is a forethrust in profile C whereas in profile A the main fault is a back thrust. The terminology of forethrust versus back thrust follows *Malavieille* [1984], where faults propagating forward in the same direction as the backstop are called forethrust and those that propagate backward relative to the backstop are called back thrust. From our results, it seems like the sedimentary load controls whether or not the main fault develops as a forethrust or back thrust. In profile C (Figure 3), the greater sedimentary load on the back thrust forced most of the deformation to localize along the forethrust. No similar conclusions can be drawn from the vergence of the main fault of the second pop-up in Figure 3. This as the sedimentary record of the basin in front of pop-up 2 is incomplete (affected by later erosion) in all profiles (A–C). Furthermore, once the orogenic wedge interferes with the pop-up, the back thrust is deactivated. This is a result of the mass increase above the hanging wall, implying higher normal stress and an increased shear stress at failure along the thrust.

4.2. Model 2

[17] In model 2A a small tilt of 0.5° toward the indenter was introduced in order to control the direction of the orogen-parallel initial river system (Figure 4a). The model was shortened 6 cm (corresponding to 60 km in 12 Myr). According to the surface transport model, 12% of the eroded material was redeposited, 88% left the model domain with the developing river system. The drainage pattern develops as a system of tributaries draining almost perpendicular to the compressive belts toward the main longitudinal river in the foreland (Figure 4a). The surface transport model did not predict any major difference in erosion or sedimentation along the rising belt and therefore erosion and sedimentation in the analogue model was applied uniformly along strike during deformation. As a consequence of this uniform erosion, no major along-strike structural changes developed. As most eroded material left the system, the deformation was affected more by erosion than by sedimentation. By the end of the experiment, a new forethrust started to develop, visible in the profile (Figure 4b).

[18] For comparison, an equivalent experiment (model 2B) was performed applying the same amount of shortening (6 cm) but involving neither erosion nor sedimentation. Here a second pop-up had formed toward the end of the experiment where both the back thrust and the forethrust were clearly visible in the profile (Figure 4c).

4.3. Model 3

[19] As in model 2, a tilt of 0.5° toward the orogenic wedge was introduced to impose an initial longitudinal

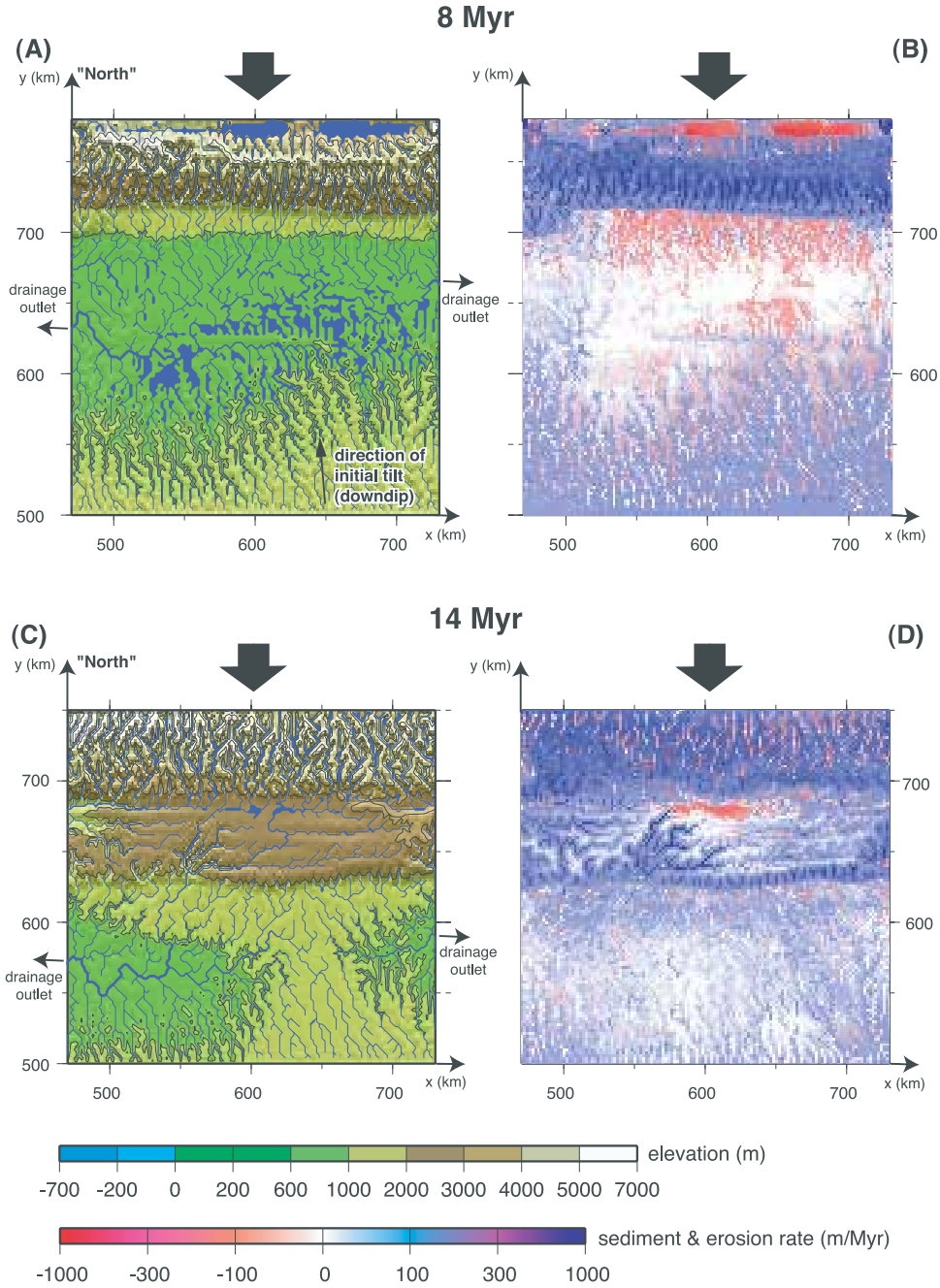

Figure 5. Model 3. (a) Resulting topography and river network and (b) erosion and sedimentation rate in m/Myr after 4 cm shortening, equivalent to 40 km shortening in 8 Myr. (c) and (d) Same as Figures 5a and 5b after 7 cm shortening (70 km, 14 Myr). Notice the effect on the drainage pattern induced by the new thrust in Figure 5c relative to the stage represented in Figure 5a. The initial topography corresponds to a plane slightly tilted (0.5°) toward the upper left direction as indicated in Figure 5a. Thick arrows indicate the movement of the rigid indenter.

(parallel to the indenter front) river network (Figure 5a). During the first 8 Myr, the surface transport model did not predict any major variations in erosion along the strike of the rising wedge even though the right side of the model started with a higher elevation due to the introduced tilt. However, the initial tilt implied drainage along a longitudinal main river in the foreland. Deposition occurred in the center of the foreland, where lakes formed on local topographic minima. Elevations in the model orogen after 8 Myr were slightly higher (~600 m) on the left side where some peaks exceeded 5000 m (Figure 5a). The calculated erosion rate at this stage was approximately uniform along strike, whereas sedimentation rates were higher on the right side (Figure 5b).

[20] After 14 Myr, elevations were still ~600 m higher on the left side, where now a large part of the wedge reached elevations exceeding 5000 m (Figure 5c). In contrast to the previous stage, relevant variations of erosion rates along the

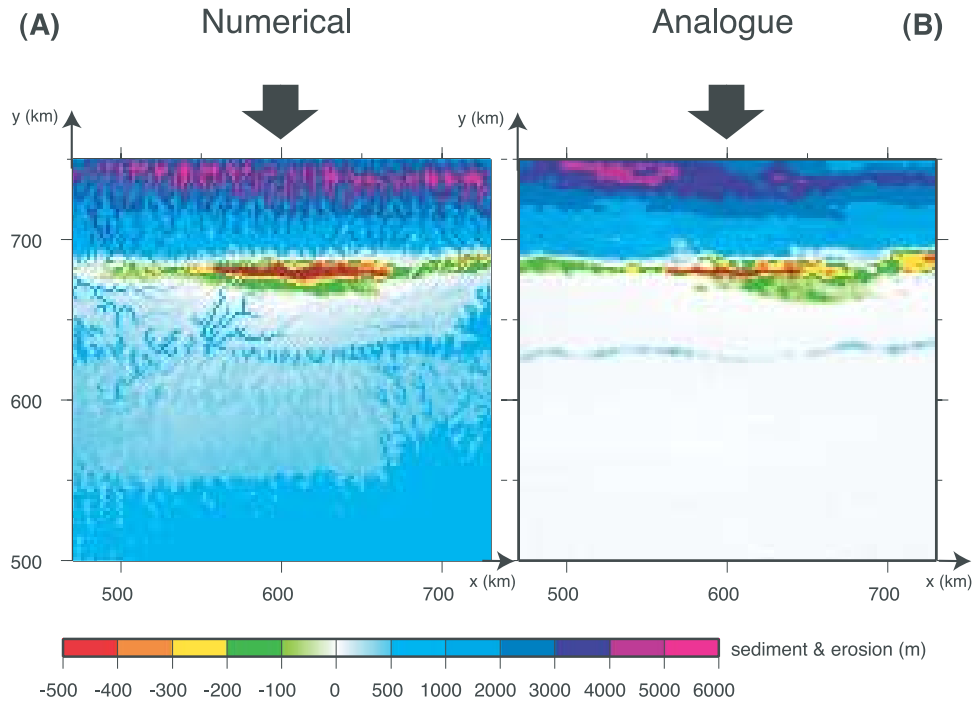

Figure 6. Model 3. (a) Spatial distribution of total cumulative erosion and sedimentation as calculated by the numerical surface transport model. (b) Erosion (sand removal) and sedimentation (sand deposition) applied to the analogue model. Thick arrows indicate the movement direction of the rigid indenter.

strike of the orogen are predicted (Figure 5d), whereas sedimentation is concentrated in front of the center of the compressional belt. These lateral variations are closely linked to the drainage patterns induced by the tectonic deformation.

[21] The total amount of removal and redeposition predicted by the numerical model and performed in the analogue model are compared in Figures 6a and 6b. The accumulated values include the thickness of every increment of erosion and deposition. Note that this indicates the total addition/subtraction of surface material at every specific x, y location relative to the stable foreland. Because the compressional belt moves as the model shortens, the values do not necessarily coincide with the exhumation undergone by particles or with the actual amount of sediment at every point. These values coincide with the sediment thickness only in the undeformed areas of the foreland. The long-wavelength differences between the predicted (numerical) and applied (analogue) erosion/sedimentation are lower than 10%, and only for wavelengths shorter than 30 km (in the scale of major river valleys) does the difference become larger than 10%.

[22] Only 4% of the eroded material is deposited within model 3. The rate of erosion increased with the amount of deformation, with three abrupt increases (at 4, 8, and 12 Myr model time), which coincided with events of high uplift rate due to thrust propagation, or with the development of new pop-up structures (Figure 7).

[23] A uniform erosion along the strike of the compressional belt resulted in an approximately uniform topography along strike in the final stage of this model (16 Myr). However, as shown in Figure 8, the main thrust of the second pop-up structure changed in vergence along strike.

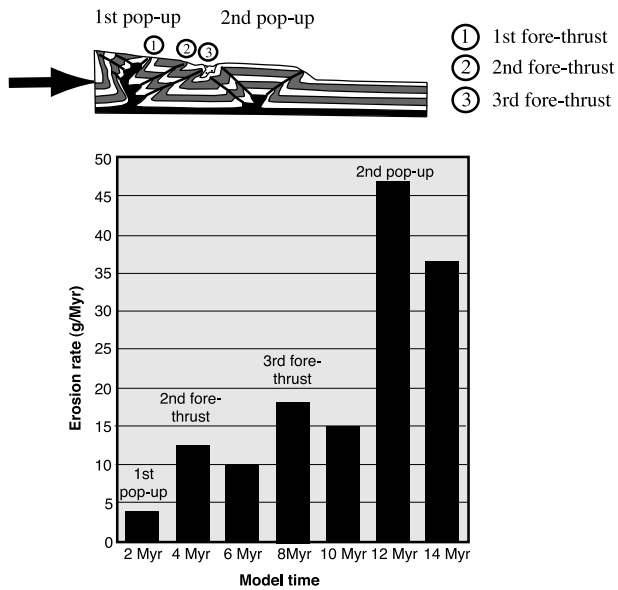

Figure 7. Erosion rates of the analogue model (sand grams per million years) over time. The rate of erosion generally increased with the amount of deformation, with three abrupt increases (at 4, 8, and 12 Myr), which coincide with events of high uplift rate due to thrust propagation or to development of new pop-up structures. The small schematic sketch of model 3 shows the corresponding structures after 14 Myr.

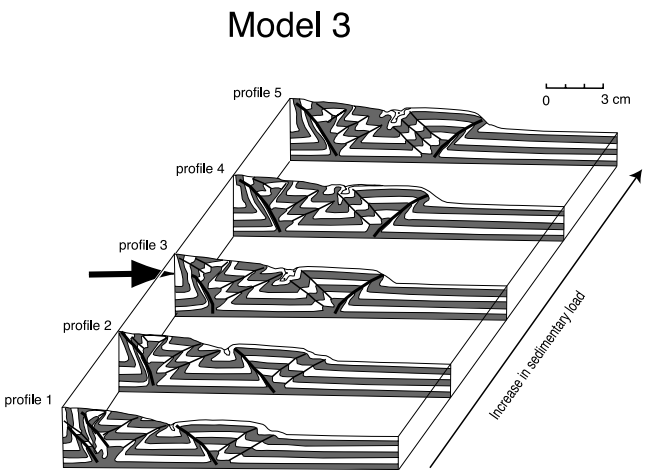

Figure 8. Cross sections of model 3 after 16 Myr. In profiles 1 and 2 the main thrusts (thicker black lines) are back thrusts, whereas in profiles 3–5 the main thrusts are forethrusts. These along-strike differences are induced by the longitudinal (orogen-parallel) variations in erosion/deposition. Dotted areas indicate sediments. Arrow indicates the movement direction of the rigid indenter.

In profiles 3–5, which experienced more sediment deposition, the main thrusts are forethrusts, while in profiles 1 and 2, the main thrusts are back thrusts.

4.4. Model 4

[24] Model 4A was also initially tilted with the same orientation and magnitude as models 2 and 3, but here an indenter (backstop) of the same vertical height as the indented sand was used to allow the sand to spread over the indenter as well as the indented sand (Figure 9). The shear plane for the back thrust developed along the front face of the indenter as a result of the similarity between the angle of internal friction of the sand (44°) and the frontal angle of the rigid indenter (30°) [cf. *Persson*, 2001]. The total shortening was 9 cm, representing 90 km in 18 Myr in the numerical transport model.

[25] The deforming model partitioned strain by developing a doubly vergent wedge with one major back thrust on top of which several consecutive forethrust were carried and deactivated as younger thrusts developed (Figure 9). The model predicts large amounts of erosion but nearly zero deposition, thus indicating that of the most erosion products left the system through the boundaries of the model. The erosion in model 4A was uniform along the strike of the compressional belt throughout the model evolution and the erosion rate generally increased with the deformation as the orogen grew in height and width. After 10 Myr, the topography had reached elevations in excess of 5000 m. Whereas the elevation of the orogen remains constant at those values after 10 Myr, its width continues to increase until the last stage of the model (18 Myr, Figure 10). The tilt initially imposed to the model was efficient in controlling the right to left flow direction of the river network on the foreland throughout the 18 Myr of deformation. The top view of the analogue model is shown in Figure 10b and the accumulated files of erosion and sedimentation can be compared in Figures 10c and 10d.

[26] For comparison, an equivalent experiment (model 4B, Figure 9) was performed involving neither erosion nor sedimentation. This model partitioned less shear strain along the back shear. We interpret this as a consequence of the higher pressure along all faults resulting from the higher (noneroded) topography. The model without erosion also developed one forethrust less than model 4A (Figure 9), instead more compaction took place within the wedge during shortening.

5. Discussion

[27] Previous studies have used analogue modeling techniques to study the role of erosion during the tectonic evolution of orogens [*Koons*, 1990; *Davy and Cobbold*, 1991; *Cobbold et al.*, 1993; *Merle and Abidi*, 1995; *Mugnier et al.*, 1997; *Persson and Sokoutis*, 2002]. Simultaneously, geomorphological studies and numerical models of landscape evolution have focused on the role of tectonics in shaping drainage patterns and surface transport of sediments [e.g., *Lin et al.*, 2001; *Kühni and Pfiffner*, 2001; *Cloetingh et al.*, 2002; *Garcia-Castellanos et al.*, 2003]. Here we integrated analogue and numerical techniques allowing for a self-consistent 3-D modeling of the interaction between both tectonics and surface transport. Numerical models provide a process-based quantitative approach to

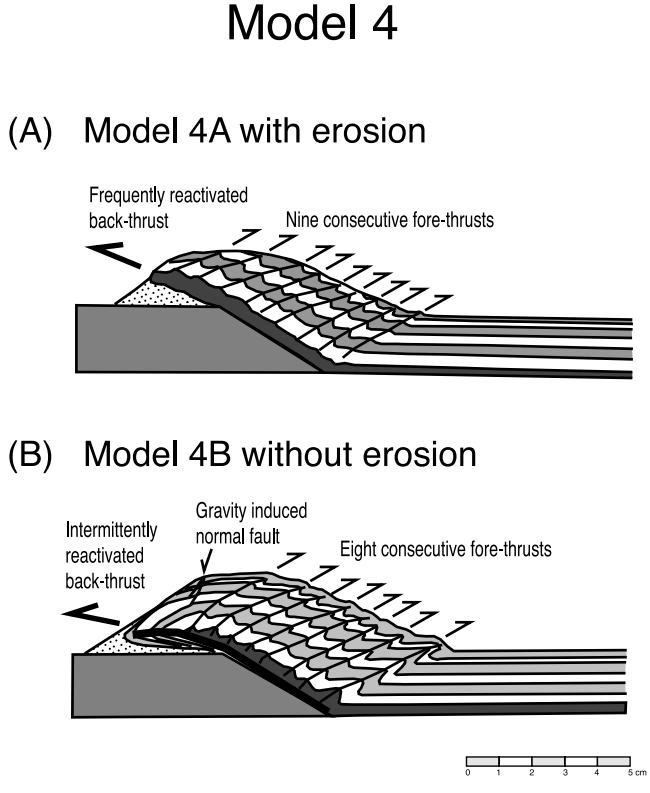

Figure 9. Model 4. Profiles after 9 cm shortening (90 km, 18 Myr) of (a) model 4A with erosion and (b) model 4B without erosion. The eroded model 4A has generated nine forethrusts, whereas model 4B without erosion has only developed eight forethrusts by the same amount of shortening. Dotted pattern represents only erosion by gravitational collapse.

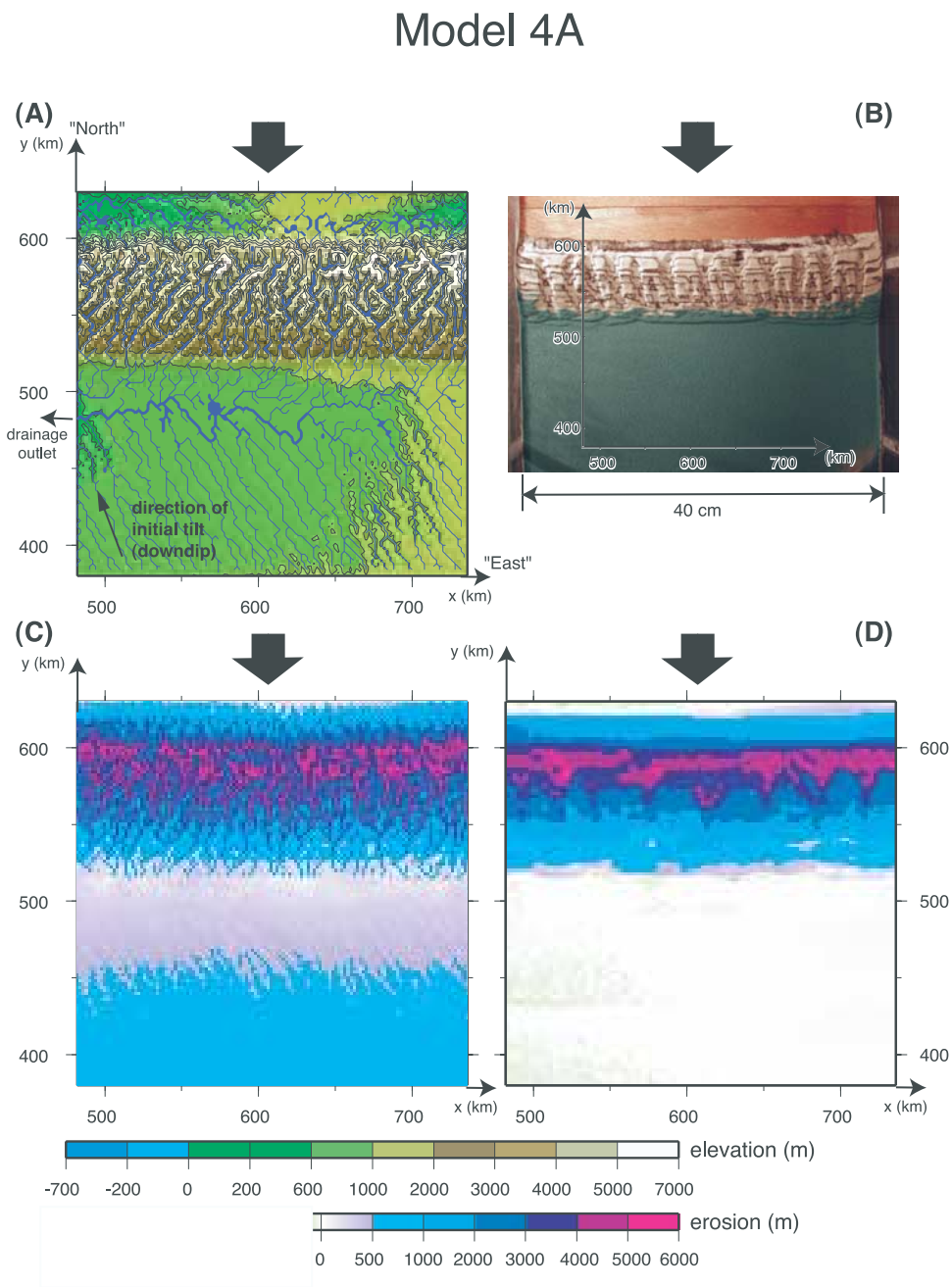

Figure 10. Model 4A with erosion after 18 Myr. (a) Topography with resulting river network. The initial topography corresponds to a plane slightly tilted (0.5°) toward the upper left direction as indicated by arrow. (b) Top view of the analogue model with the coordinate system corresponding to the numerical model. (c) Total erosion calculated by the numerical surface transport model. (d) Total erosion applied to the analogue model. Thick arrows indicate the direction of shortening of the model.

predict the amount and spatial distribution of erosion and sedimentation, as a function of the evolution of active topography. Our analogue models incorporate the predicted lateral and temporal variations of erosion and sedimentation, rather than assuming them a priori. However, the models above still incorporate some simplifications that need to be considered. They do not take into account the flexural foreland basin that would normally develop in front of a compressional belt. This leads to underestimation of sedimentation within the model as most erosion products leave the system. Model 4 is a clear example of this, where all eroded sediments were carried out of the model domain, according to the surface transport model. In spite of this, the sediment distribution appears to control the lateral changes in the tectonic evolution of both models 1 and 3. The additional load of sediments deposited in front of these compressional belts controlled the vergence of the main thrust as well as the forward propagation of later thrust wedges. A flexural basin would also enhance the lateral (orogen-parallel) asymmetry along the compressional belt, as the additional

sediment load would lead to further widening of the thrust wedge (compare model 1 with enhanced sedimentation on one side). Finally, incorporating regional isostasy to the model, would also avoid the need for a vertical scale smaller than the horizontal scale.

[28] The sedimentary load also controls whether or not the compressional belt partitions strain along a main forethrust or a main back thrust. In model 3, the sedimentary load on the back side of the second pop-up wedge in profiles 3–5 (Figure 8) forced the model to strain partition by slip, mainly along a single reactivated forethrust. Where the sedimentary load is lower (profiles 1–2 in Figure 8), a back thrust acts as the main shear. In comparison, four-layer analogue models by *Davy and Cobbold* [1991] and *Cobbold et al.* [1993] develop footwall flexures, resulting in foreland basins that are also seen to be further accentuated by sedimentation [*Cobbold et al.*, 1993]. However, in contrast to our approach, their work did not provide a quantitative control of the surface mass transport. We strongly believe that integrating both flexural basin formation and quantitative approaches of erosion/sedimentation would significantly improve our understanding of the role of surface processes on lithospheric scale deformation.

[29] Taking into account the limitations discussed above, the effects of erosion are more relevant than that of sediment accumulation in our models. Erosion rate controls the lifetime of individual faults as well as the degree of rotation of the faults as the entire wedge undergoes internal deformation. It is generally accepted, that the criticality of the wedge is disturbed by the removal of load above faults [cf. *Jamieson and Beaumont*, 1988, 1989]. However, erosion cannot be related directly to the development of fewer forethrusts for the same amount of erosion. In model 4, nine closely spaced forethrusts developed, all traveling up a single, periodically reactivated back thrust (Figure 9a). In a similar model, after the same amount of shortening but without erosion, only eight forethrust developed (Figure 9b). However, the back thrust in the model without erosion, was not extruding material as efficiently as the model with erosion. Erosional unloading of sand from above the thrust made it easier for the model to partitioning strain by shear along this back thrust while simultaneously forming conjugate forethrusts, instead of accommodating shortening by compaction [cf. *Persson and Sokoutis*, 2002]. This is in agreement with previous field and model studies that show high extrusion rates along erosionally unloaded faults, exposing high-grade metamorphic rocks at the surface [*Koons*, 1990; *Norris and Cooper*, 1997; *Persson and Sokoutis*, 2002].

[30] The rates of erosion and sedimentation calculated by the numerical model were not constant over time. In overall, the quantified erosion rate and sedimentation rate increased as the wedge grew during deformation. Both erosion and sedimentation rates peaked soon after the development of new thrusts or reactivation of older thrusts, i.e., events that resulted in uplift (Figure 7). Peaks in surface mass transport occur in the models despite the shortening rate being constant. These peaks are related to phases of uplift when strain is accommodated by slip along imbricate thrust planes rather than by slip along basal décollements or lateral compaction. The results from the integrated models strongly question the necessity of attributing peaks in sediment delivery to discrete shortening events during orogenesis.

6. Conclusions

[31] 1. The integration of numerical surface transport models with analogue models provides a powerful tool to further study the interplay between surface transport and tectonic deformation.

[32] 2. High erosion rates do not always lead to fewer thrusts but generally expand the lifetime of thrusts. High erosion rates promote the accommodation of strain by shear along back thrusts while simultaneously forming conjugate forethrusts, thus increasing the number of total thrusts and reducing shortening accommodation by compaction.

[33] 3. The pattern of tectonic deformation in the analogue orogen determines the orogen-parallel fluvial transport in the foreland, which in turn induces strong spatial variations in erosion and deposition. Inversely, these along-strike differences in the erosion/sedimentation balance influence the style of tectonic deformation of the analogue orogen.

[34] 4. Constant convergence rates in orogens do not necessarily imply that fluvial transport is uniform in time. Peaks of erosion and sedimentation rate can result from changes in strain partitioning, producing periods of relative high uplift rates. Care will be needed to distinguish climatic from tectonic signals in syntectonic proximal sediments.

[35] **Acknowledgments.** Katarina's research visit to the Vrije Universiteit (Amsterdam) was financed by Gertrud Thelin's travel grant from Uppsala University. We are grateful to S. Cloetingh and the Netherlands Centre for Integrated Solid Earth Science (ISES) tectonic laboratory at Vrije Universiteit, Amsterdam, for providing the necessary infrastructure. Many thanks to C. J. Talbot and G. Mulugeta for comments on both science and English. J. H. W. Smit is kindly thanked for technical advice. We also thank the reviewers David Burbidge and Adrian Pfiffner for their constructive criticism that greatly improved the manuscript. Dimitrios Sokoutis and Daniel Garcia-Castellanos kindly acknowledge the financial support from ISES and Netherlands Organization for Scientific Research (NWO).

References

Ahnert, F. (1970), Functional relationships between denudation, relief, and uplift in large mid-latitude drainage basins, *Am. J. Sci*, *268*, 243–263.

Avouac, J. P., and E. B. Burov (1996), Erosion as a driving mechanism of intracontinental mountain growth, *J. Geophys. Res.*, *101*(B8), 17,747–17,769.

Barry, R. G. (1981), *Mountain Weather and Climate*, 313 pp., Methuen, New York.

Beaumont, C., P. Fullsack, and J. Hamilton (1992), Erosion control of active compressional orogens, in *Thrust Tectonics*, edited by K. R. McClay, pp. 1–18, Chapman and Hall, New York.

Beaumont, C., R. A. Jamieson, M. H. Nguyen, and B. Lee (2001), Himalayan tectonics explained by extrusion of a low-viscosity crustal channel coupled to focused surface denudation, *Nature*, *414*, 738–742.

Bonini, M., D. Sokoutis, C. J. Talbot, M. Boccaletti, and A. G. Milnes (1999), Indenter growth in analogue models of Alpine-type deformation, *Tectonics*, *18*, 119–128.

Byerlee, J. (1978), Friction of rocks, *Pure Appl. Geophys.*, *116*, 615–626.

Cloetingh, S., E. Burov, F. Beekman, B. Andeweg, P. A. M. Andriessen, D. Garcia-Castellanos, G. de Vicente, and R. Vegas (2002), Lithospheric folding in Iberia, *Tectonics*, *21*(5), 1041, doi:10.1029/2001TC901031.

Cobbold, P. R., P. Davy, D. Gapais, E. A. Rossello, E. Sadybakasov, J. C. Thomas, J. J. Tondji Bijo, and M. de Urreiztieta (1993), Sedimentary basins and crustal thickening, *Sediment. Geol.*, *86*, 77–89.

Davis, D., J. Suppe, and F. A. Dahlen (1983), Mechanism of fold-and-thrust belts and accretionary wedges, *J. Geophys. Res.*, *88*, 1153–1172.

Davy, P., and P. R. Cobbold (1991), Experiments on shortening of a 4-layer model of the continental lithosphere, *Tectonophysics*, *188*, 1–25.

Garcia-Castellanos, D. (2002), Interplay between lithospheric flexure and river transport in foreland basins, *Basin Res.*, *14*, 89–104.

Garcia-Castellanos, D., J. Verges, J. M. Gaspar-Escribano, and S. Cloetingh (2003), Interplay between tectonics, climate and fluvial transport during the Cenozoic evolution of the Ebro Basin (NE Iberia), *J. Geophys. Res.*, *108*(B7), 2347, doi:10.1029/2002JB002073.

Goodman, R. E. (1989), *Introduction to Rock Mechanics*, 2nd ed., 562 pp., John Wiley, Hoboken, N. J.

Gupta, S. (1997), Himalayan drainage patterns and the origin of fluvial megafans in the Ganges foreland basin, *Geology*, *25*, 11–14.

Hoffman, P. F., and J. P. Grotzinger (1993), Orographic precipitation, erosional unloading, and tectonic style, *Geology*, *21*, 195–198.

Howard, A. D. (1994), A detachment-limited model of drainage basin evolution, *Water Resour. Res.*, *30*, 2261–2285.

Jamieson, R. A., and C. Beaumont (1988), Orogeny and metamorphism: A model for deformation and P-T-t paths with applications to the central and southern Appalachians, *Tectonics*, *7*, 417–445.

Jamieson, R. A., and C. Beaumont (1989), Deformation and metamorphism in convergent orogens: A model for uplift and exhumation of metamorphic terrains, in *Evolution of Metamorphic Belts*, edited by J. S. Daly, R. A. Cliff, and B. W. D. Yardly, Geol. Soc. Spec. Publ., *43*, 117–129.

Kooi, H., and C. Beaumont (1996), Large-scale geomorphology: Classical concepts reconciled and integrated with contemporary ideas via a surface process model, *J. Geophys. Res.*, *101*, 3361–3386.

Koons, P. O. (1990), Two-sided orogen: Collision and erosion from sandbox to the Southern Alps, New Zealand, *Geology*, *18*, 679–682.

Kühni, A., and O. A. Pfiffner (2001), Drainage patterns and tectonic forcing: A model study for the Swiss Alps, *Bas. Res.*, *13*, 169–197.

Kusznir, N. J., and R. G. Park (1984a), Intraplate lithosphere deformation and the strength of the lithosphere, *Geophys. J. R. Astron. Soc.*, *79*, 513–538.

Kusznir, N. J., and R. G. Park (1984b), The strength of intraplate lithosphere, *Phys. Earth Planet. Inter.*, *36*, 224–235.

Leturmy, P., J. L. Mugnier, P. Vinour, P. Baby, B. Colletta, and E. Chabron (2000), Piggyback basin development above a thin-skinned thrust belt with two detachment levels as a function of interactions between tectonic and superficial mass transfer: The case of the Subandean Zone (Bolivia), *Tectonophysics*, *320*, 45–67.

Lin, A., Z. Yang, Z. Sun, and T. Yang (2001), How and when did the Yellow River develop its square bend?, *Geology*, *29*, 951–954.

Malavieille, J. (1984), Modélisation expérimentale des chevauchements imbriqués: Application aux chaînes de montagnes, *Bull. Soc. Geol. Fr.*, *7*, 129–138.

Merle, O., and N. Abidi (1995), Approche expérimentale du fonctionnement des rampes émergentes, *Bull. Soc. Geol. Fr.*, *166*, 439–450.

Mugnier, J. L., P. Baby, B. Colletta, P. Vinoue, P. Bale, and P. Leturmy (1997), Thrust geometry controlled by erosion and sedimentation: A view from analogue models, *Geology*, *25*, 427–430.

Norris, R. J., and A. F. Cooper (1997), Erosional control on the structural evolution of a transpressional thrust complex on the Alpine fault, New Zealand, *J. Struct. Geol.*, *19*, 1323–1342.

Persson, K. S. (2001), Effective indenters and the development of double-vergent orogens: Insights from analogue sand models, in *Tectonic Modeling: A Volume in Honor of Hans Ramberg*, edited by H. A. Koyi and N. S. Mancktelow, *Mem. Geol. Soc. Am.*, *193*, 191–206.

Persson, K. S., and D. Sokoutis (2002), Analogue models of orogenic wedges controlled by erosion, *Tectonophysics*, *356*, 323–336.

Pfiffner, O. A., S. Ellis, and C. Beaumont (2000), Collision tectonics in the Swiss Alps: Insight from geodynamic modeling, *Tectonics*, *19*, 1065–1094.

Ruddiman, W. F. (1997), *Tectonic Uplift and Climate Change*, 535 pp., Plenum, New York.

Schlunegger, F., J. Melzer, and G. E. Tucker (2001), Climate, exposed source-rock lithologies, crustal uplift and surface erosion: A theoretical analysis calibrated with data from the Alps/North Alpine Foreland Basin system, *Int. J. Earth Sci.*, *90*, 484–499.

Schmid, S. M., O. A. Pfiffner, N. Froitzheim, G. Schönborn, and E. Kissling (1996), Geophysical-geological transect and tectonic evolution of the Swiss-Italian Alps, *Tectonics*, *15*, 1036–1064.

Sonder, L. J., and P. England (1986), Vertical averages of rheology of the continental lithosphere: Relation to thin sheet parameters, *Earth Planet. Sci. Lett.*, *77*, 81–90.

Tucker, G. E., and R. L. Slingerland (1997), Drainage responses to climate change, *Water Resour. Res.*, *33*, 2031–2047.

Weijermars, R., and H. Schmeling (1986), Scaling of Newtonian and non-Newtonian fluid dynamics without inertia for quantative modeling of rock flow due to gravity (including the concept of rheological similarity), *Phys. Earth Planet. Inter.*, *43*, 316–330.

Whipple, K. X., and G. E. Tucker (1999), Dynamics of the stream-power river incision model; implications for height limits of mountain ranges, landscape response timescales, and research needs, *J. Geophys. Res.*, *104*, 17,661–17,674.

Willett, S. D. (1999), Orogeny and orography: The effects of erosion on the structure of mountain belts, *J. Geophys. Res.*, *104*, 28,957–28,981.

Willett, S. D., and M. T. Brandon (2002), On steady states in mountain belts, *Geology*, *30*, 175–178.

D. Garcia-Castellanos and D. Sokoutis, Netherlands Centre for Integrated Solid Earth Science, Faculty of Earth and Life Sciences, Vrije Universiteit Amsterdam, De Boelelaan 1085, 1081 HV, Amsterdam, Netherlands.

K. S. Persson, Geological Survey of Sweden, Box 670, 751 28 Uppsala, Sweden. (katarina.persson@sgu.se)